

Exploring a Hybrid Deep Learning Approach for Anomaly Detection in Mental Healthcare Provider Billing: Addressing Label Scarcity through Semi-Supervised Anomaly Detection

Samirah Bakker¹, Yao Ma^{1*}, Seyed Sahand Mohammadi Ziabari^{1,2}

¹Informatics Institute, University of Amsterdam, 1098XH Science Park, Amsterdam, The Netherlands

²Department of Computer Science and Technology, SUNY Empire State University, Saratoga Springs, NY, USA
samirah.bakker@student.uva.nl, y.ma3@uva.nl, sahand.ziabari@sunyempire.edu

ABSTRACT

The complexity of mental healthcare billing enables anomalies, including fraud. While machine learning methods have been applied to anomaly detection, they often struggle with class imbalance, label scarcity, and complex sequential patterns. This study explores a hybrid deep learning approach combining Long Short-Term Memory (LSTM) networks and Transformers, with pseudo-labeling via Isolation Forests (iForest) and Autoencoders (AE). Prior work has not evaluated such hybrid models trained on pseudo-labeled data in the context of healthcare billing. The approach is evaluated on two real-world billing datasets related to mental healthcare. The iForest LSTM baseline achieves the highest recall (0.963) on declaration-level data. On the operation-level data, the hybrid iForest-based model achieves the highest recall (0.744), though at the cost of lower precision. These findings highlight the potential of combining pseudo-labeling with hybrid deep learning in complex, imbalanced anomaly detection settings.

KEYWORDS

Anomaly detection, Deep learning, Hybrid models, Mental healthcare, Pseudo-labeling

1 INTRODUCTION

The complexity of healthcare billing and large insurance volumes create an environment where anomalies, including fraud, can thrive [16]. Fraud by healthcare providers results in significant financial losses and negatively impacts healthcare systems [32]. In the Netherlands, healthcare fraud is estimated to cost billions of euros annually [3], burdening insurers. Despite ongoing efforts, the likelihood of identifying perpetrators remains low, underscoring the need for more effective detection methods.

Mental healthcare billing, in particular, has proven vulnerable to fraud due to the complexity of diagnoses and treatments, as well as the difficulty of verifying the provided services. Investigations have exposed fraudulent practices, including billing for unprovided claims, inflated rates, and double-charging for services [28, 41]. These cases highlight the urgent need for fraud detection methods to prevent financial abuse.

A fundamental challenge in fraud detection is the highly imbalanced data, where normal transactions significantly outnumber fraudulent cases. This imbalance often leads to performance bias [7], especially since labeled fraud cases are typically scarce in practical applications [31]. In this context, fraud can be framed as an anomaly detection problem, where the goal is to find rare patterns in the data that deviate from the expected behavior. To address these

challenges, this study adopts a pseudo-labeling strategy based on unsupervised anomaly detection. Instead of relying on a small number of labeled fraud cases, unsupervised models identify structural deviations in the data to generate synthetic labels, thereby enriching the minority class. Recent studies have shown that such strategies can enhance classification performance across multiple domains where labeled data is scarce [14, 17, 25].

Although widely used, machine learning methods face increasing challenges as fraudulent techniques evolve and high-dimensional data grows. As a result, these methods struggle to identify these anomalies over time [44]. By contrast, deep learning models have consistently outperformed conventional machine learning algorithms in fraud detection tasks due to their ability to learn complex, high-dimensional relationships [4, 21]. In particular, Long Short-Term Memory (LSTM) networks are well-suited for detecting temporal anomalies in sequential data [30]. In addition, Transformers, due to their self-attention mechanism, can effectively capture complex dependencies and interactions within the data [50]. Their robust performance across domains has been demonstrated in various anomaly detection tasks. Combining these two approaches can offer an even more effective solution, as it builds on the strengths of each model. While LSTMs and Transformers have been applied separately for anomaly detection, their combined use remains largely unexplored in the context of imbalanced mental healthcare billing data. Moreover, the application of pseudo-labeling with hybrid models in this domain is understudied.

This study proposes a hybrid deep learning framework that combines LSTM networks and Transformer architectures to improve anomaly detection in imbalanced mental healthcare billing data. The approach addresses key challenges in this domain, including data imbalance, limited labeled instances of anomalous behavior, and the complex temporal and contextual patterns inherent in billing sequences.

To mitigate the issue of label scarcity, the methodology incorporates pseudo-labeling strategies using unsupervised anomaly detection techniques such as Isolation Forests and Autoencoders. These methods generate synthetic anomaly labels to augment the training data, allowing the hybrid model to learn from enriched and more representative datasets. The integration of LSTM and Transformer components enables the model to capture both temporal dependencies and intricate feature interactions, making it particularly suitable for complex anomaly detection tasks.

The proposed framework is evaluated on two real-world datasets drawn from mental healthcare provider billing systems. Experimental results demonstrate that pseudo-labeling significantly enhances

model performance across several metrics. In particular, the hybrid model outperforms standalone LSTM or Transformer architectures in detecting irregularities in both declaration- and operation-level data, achieving higher recall in scenarios where precision trade-offs are acceptable.

This work contributes to the literature by demonstrating the viability of combining pseudo-labeling with hybrid deep learning architectures for anomaly detection in complex, high-dimensional, and imbalanced healthcare billing environments. The findings underscore the importance of architecture design and data enrichment strategies in building robust anomaly detection systems where labeled data is limited or incomplete.

The remainder of this study is organized as follows: Section 2 presents a review of related work, while Section 3 details the methodology. Section 4 presents the results followed by a discussion on the findings and implications in Section 5. Finally, Section 6 provides concluding remarks.

2 RELATED WORK

Fraud detection is a well-studied application of anomaly detection, where the goal is to correctly classify rare instances that deviate from expected patterns. Despite ongoing advancements, multiple challenges remain, such as annotation delays and constantly evolving fraud patterns [11]. Additionally, the highly imbalanced nature of fraud datasets, with fraudulent transactions comprising only about 0.2% of total transactions, remains a significant challenge [22]. This section reviews existing machine learning and deep learning approaches for anomaly detection, discusses recent advances in hybrid models, and introduces pseudo-labeling for addressing class imbalance. In doing so, it highlights the research gaps this study aims to address.

2.1 Machine learning models

Many machine learning methods, such as supervised learning, learn patterns from historical data. However, they often struggle with high-dimensional and sequential data, real-time fraud detection, and imbalanced datasets, where anomalies affect a small percentage of the data [10, 33]. For instance, Jain et al. [20] found that Artificial Neural Networks (ANN) achieved 99.71% accuracy in credit card fraud detection. However, they noted that most fraud detection techniques struggle with real-time detection due to the rarity of fraud, often identifying it post-occurrence. Similarly, Sailusha et al. [37] achieved 99.91% accuracy with Random Forest and AdaBoost but faced high false negative rates, advocating for deep learning to improve detection and reduce misclassification. Raghavan and Gayar [34] showed that Support Vector Machines (SVM) performed best on larger datasets, while Convolutional Neural Networks (CNN) outperformed other deep learning models. Nevertheless, the lack of suitable training data remained a major challenge. Although these methods have shown some success, they struggle to capture the complex and evolving patterns of anomalies in sequential data. These limitations underscore the need for more advanced and flexible approaches to fraud detection.

2.2 Deep learning models

A promising area for improving anomaly detection is the use of deep learning models. These models excel at processing high-dimensional data and capturing non-linear relationships, making them well-equipped to identify subtle and hidden patterns that traditional methods often miss [31]. For more complex tasks like fraud detection, deep learning algorithms generally outperform conventional machine learning algorithms [4].

2.2.1 Recurrent Neural Networks. Among deep learning models, Recurrent Neural Networks (RNN), such as LSTM models, have shown potential in modeling sequential data [40, 48]. Their ability to process high-dimensional, time-dependent data provides an advantage for anomaly detection in complex, real-time environments. RNNs have especially proven effective at handling the complexities of financial transaction data, as demonstrated by Dutta and Bandyopadhyay [15]. They proposed a stacked RNN model to monitor and detect fraudulent financial transactions in mobile money systems, which achieved an accuracy of 99.87%. Similarly, Rosaline et al. [36] used an LSTM-RNN for credit card fraud detection, incorporating an attention mechanism to enhance performance. Their results demonstrated the effectiveness of LSTM-RNN in handling complex and interrelated data, outperforming classifiers like Naive Bayes, SVM, and ANN. Benchaji et al. [6] further highlighted the potential of LSTM models for fraud detection by integrating an attention mechanism as well as uniform manifold approximation and projection for feature selection. Their experimental results demonstrated that their model outperformed traditional methods.

Despite improvements such as attention mechanisms, RNNs still face challenges when it comes to understanding long-range dependencies and processing large-scale datasets efficiently [30]. In addition, traditional RNNs suffer from the vanishing gradient problem, which makes it difficult for these models to retain information over long sequences. This leads to a loss of context and reduced performance [43].

2.2.2 Transformers. Transformers overcome these challenges by processing entire sequences simultaneously. With their self-attention mechanism, Transformers can capture correlations by assigning different weights to different sections of the input sequence. Their robust performance across various tasks has been successfully applied to multiple domains, including anomaly detection. Transformers have shown great promise, as seen in the work of Tang et al. [44], who applied a Transformer-based model for financial fraud detection, outperforming traditional machine learning methods. Taneja et al. [42] also proposed a Transformer-based framework using BERT for online recruitment fraud detection. Their model demonstrated superiority over conventional methods, achieving an accuracy score of 99%. Yu et al. [50] further demonstrated the effectiveness of Transformer models in credit card fraud detection, highlighting their advanced capability to improve accuracy and robustness. Their experimental results showed that the Transformer outperformed traditional methods, showcasing their potential in anomaly detection.

Nevertheless, a known limitation of Transformers is their quadratic memory complexity within the self-attention mechanism, which can lead to scalability issues. This can be problematic in

anomaly detection, where large sequential datasets need to be processed. While both RNNs and Transformers have individual strengths, solely relying on a single model is not sufficient to fully capture the complexities of fraudulent activities.

2.2.3 Hybrid models. To mitigate the limitations of individual architectures, recent studies have explored the effectiveness of hybrid approaches that combine RNNs with Transformers. For instance, Zhou et al. [51] demonstrated the potential of these models for multiscanning-based hyperspectral image classification, achieving competitive classification performance. Furthermore, Riaz et al. [35] applied a hybrid LSTM-Transformer model for fine-grained suggestion mining, showing its ability to enhance the quality and relevance of mined suggestions. In the context of anomaly detection, Ileberi and Sun [18] successfully combined LSTM, CNN, and Transformers to enhance credit card fraud detection. Their hybrid approach outperformed individual-based learners and traditional methods. By leveraging the strength of each model, they were able to capture both spatial and temporal patterns as well as complex relationships within the data.

However, to the best of the authors’ knowledge, the combination of RNNs and Transformer models for anomaly detection has not yet been explored. Building on previous work, this study proposes a more focused hybrid approach, combining only LSTM and Transformer models. By simplifying the ensemble to only two models, this research aims to reduce complexity while still leveraging the complementary strengths of LSTMs for sequential data processing and Transformers for capturing intricate feature interactions in transaction data.

2.3 Pseudo-labeling

Pseudo-labeling has emerged as a practical approach to mitigate class imbalance in anomaly detection. A common strategy is to apply semi-supervised learning, where a small set of labeled anomalies is used to create pseudo-labels. However, this approach risks producing biased models since it heavily relies on a small amount of labeled data when there is a distribution mismatch between the labeled and unlabeled data [49]. Unsupervised strategies address this issue by identifying outliers based on structural deviations present in the data itself, rather than relying on labeled data.

Prior work has demonstrated that unsupervised pseudo-labeling methods can enhance anomaly detection performance in highly imbalanced datasets. For instance, Al-Lahham et al. [2] introduced a coarse-to-fine pseudo-labeling framework that identifies anomalous video segments based on the statistical properties of the data. Similarly, Im et al. [19] proposed an unsupervised method that refines pseudo-labels by only using internal data consistency, showing strong results in highly imbalanced settings. Unlike techniques such as SMOTE or random oversampling, which assume a well-defined distribution of the minority class and may introduce noise, pseudo-labeling leverages the inherent structure of the data. This makes it particularly suitable for domains like mental healthcare billing, where anomalies are rare and often unlabeled.

Although pseudo-labeling has shown promise for minority class enrichment, its combination with hybrid learning models is still underexplored. This study addresses this gap by evaluating an LSTM-Transformer hybrid model trained on pseudo-labeled mental

healthcare billing data. Beyond fraud detection in mental healthcare, recent studies have highlighted the broader applicability of deep learning and data strategies for anomaly detection. Deshamudre et al. [12] emphasized the role of structured data preparation and neural architectures in enhancing heart disease prediction accuracy. Similarly, Chatterjee et al. [9] explored the performance and ethical dimensions of machine learning-based fraud detection in payment systems, highlighting the importance of explainability and domain alignment. These works support the relevance of combining data strategies and model selection when addressing complex, high-stakes anomaly detection problems.

3 METHODOLOGY

This study evaluates a hybrid anomaly detection model for imbalanced mental healthcare billing data. It combines an LSTM, a Transformer, and a meta-learner to aggregate their predictions. This section outlines the dataset, pre-processing, pseudo-label generation via unsupervised anomaly detection, model implementation, and performance evaluation methods. Figure 1 illustrates the hybrid model pipeline.

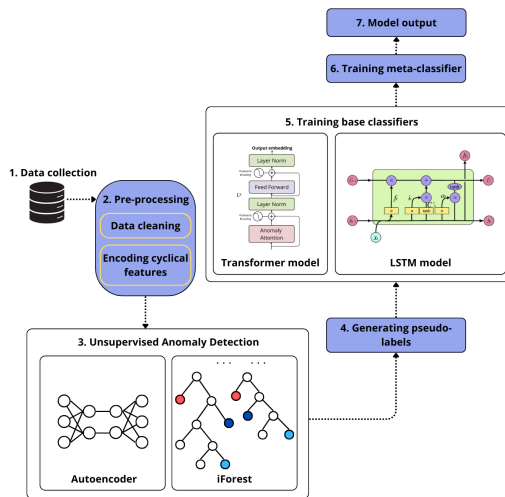


Figure 1: Overview of the hybrid model pipeline for anomaly detection. The process includes data collection, pre-processing, and unsupervised anomaly detection. Detected anomalies generate pseudo-labels for training base classifiers, whose predictions are combined by a meta-classifier to produce the final output.

3.1 Datasets

The datasets used in this study were obtained through a collaboration and comprise two proprietary real-world datasets: one at the declaration-level and the other at the operation-level. Both contain anonymized financial metadata from mental healthcare providers. Each dataset includes binary fraud labels, indicating whether a record has been flagged as fraudulent.

The declaration-level dataset consists of 74,699 billing records across 16 variables from March 2022 to March 2025. The records

include invoice amounts, accepted claims, insured coverage, and metadata such as submission dates, payment terms, and early payment requests. One confirmed fraud case was identified before receiving the datasets, involving 349 billing records linked to a single client out of 202 total clients.

The operation-level dataset contains 1,593,647 records across 24 variables, covering operation-level billing records from March 2022 to mid-April 2025. It links individual operations to their corresponding declarations and includes treatment codes, claim rejections, and submission dates. It covers the same 202 clients and 1,799 unique mental healthcare practitioners. The known fraudulent client appears in up to 84 operations tied to a single declaration, with an average of two unique operations per declaration overall.

3.2 Pre-processing

With already aligned units, both datasets were cleaned of erroneous entries, normalized, and encoded for cyclical features. NaN values and non-positive billing amounts were removed, resulting in 71,196 entries and 16 columns for the declaration-level dataset and 1,589,951 entries and 24 columns for the operation-level dataset. Other outliers were retained, as they may indicate fraudulent behavior.

3.2.1 Encoding cyclical features. Temporal features were transformed into two dimensions using sine and cosine transformations to capture cyclical patterns. These transformations map each time-related value to a corresponding point in a unit circle, ensuring continuity between the start and end of each cycle. This approach aligns with recent studies on time series data pre-processing for machine learning models [38, 45]. The date time column was split into year, month, day of week, day, hour, minute, and second. The year variable was retained as a numerical feature since years do not exhibit cyclical behavior. To capture the cyclic nature of these features, they were encoded using the following equations:

$$\begin{aligned} x_{sin} &= \sin\left(\frac{2 \cdot \pi \cdot x}{\max(T)}\right) \\ x_{cos} &= \cos\left(\frac{2 \cdot \pi \cdot x}{\max(T)}\right) \end{aligned} \quad (1)$$

Where x is the cyclical feature (e.g., hour or day) and $\max(T)$ is the maximum value for a certain cycle (e.g., 24 hours).

3.2.2 Feature scaling and encoding. All numerical features were normalized using Min-Max scaling to ensure stable training for gradient-based models, such as LSTMs and Transformers. Furthermore, to enable quantitative representation, all categorical features were one-hot encoded. In both datasets, the payment term (1-6 weeks) and file rejection reason were one-hot encoded, resulting in seven new features.

3.2.3 Sliding window. To enable sequential modeling, a fixed-length sliding window approach was applied. Each window contained chronologically ordered features and was labeled by its final timestep. Exploratory data analysis showed cyclical and repetitive billing behavior, supporting the use of sliding windows to capture temporal dependencies. Data was sorted chronologically to preserve temporal order. Sliding windows were extracted from the full dataset without grouping by entity, allowing the model to learn global

patterns. Shorter sequences were removed to avoid zero-padding, which could distort learning. A default window size of 100 was used to capture long-range dependencies. For the LSTM and Transformer models trained on pseudo-labeled operation-level data, a window size of 50 was applied. This reduced dimensionality and improved performance based on empirical testing. In contrast, the original-label model used size 100, as extreme class imbalance required the model to leverage more temporal context to detect subtle anomalies.

3.3 Unsupervised anomaly detection

The original binary fraud labels were excluded from all modeling steps due to extreme class imbalance, with only 0.4% of instances labeled as anomalous. To address this, this study adopted an unsupervised pseudo-labeling approach based on anomaly techniques. This strategy identifies outliers from structural deviations present in the data without relying on labels. All pseudo-labels were derived from the original datasets, without introducing any synthetic anomalies. Two distinct unsupervised models were applied to generate pseudo-labels: Isolation Forest (iForest) and Autoencoder (AE). Both models were trained on the declaration-level and operation-level datasets, enabling comparison of their effectiveness. The pseudo-codes for the iForest and AE pseudo-labeling models are presented in Algorithm 1 and Algorithm 2. Label quality was visually validated using t-SNE and density plots, and agreement between the two models was inspected to assess consistency.

3.3.1 Isolation Forest. iForest, known for its effectiveness in anomaly detection and scalability on large datasets, was used for pseudo-labeling. iForest is particularly well-suited for high-dimensional data, where it isolates anomalies by partitioning data points within an ensemble of random isolation trees. Anomalies are expected to be isolated more quickly, which results in shorter average path lengths. iForest is robust to outliers and can effectively isolate anomalies even in complex and non-linear datasets [24, 26, 46]. Instances received anomaly scores between -1 and 1, where negative values indicate outliers and positive values indicate inliers. Data points originally labeled as non-fraud but exceeding a defined anomaly score threshold θ were assigned a pseudo-label of 1.

3.3.2 Autoencoder. A limitation of iForest is its reliance on a tree-based approach, which can struggle to capture more complex anomaly patterns, as each isolation operation considers only one feature at a time [46]. To address this limitation, AE has been applied as a separate method for anomaly detection and pseudo-labeling. AE is an unsupervised artificial neural network consisting of an input layer, a hidden layer, and an output layer. It operates through an encoder-decoder structure, where the encoder reduces the initial input data by mapping it to a hidden representation with a smaller dimension. The decoder reconstructs the original input from this compressed form. The main objective of an AE is to minimize the reconstruction error [1]. Anomalous instances, which differ from the majority of the data, typically exhibit higher reconstruction errors due to their dissimilarity to the learned normal patterns. By generating pseudo-labels based on the reconstruction error, AE offers a complementary method to iForest for capturing more complex anomaly patterns that iForest might miss.

Algorithm 1: Isolation Forest for pseudo-labeling

Input: $X = \{x_1, x_2, \dots, x_n\}$ - Input dataset with n instances
Input: T - Number of isolation trees
Input: c - Contamination rate
Output: Pseudo-labeled data with labels y_i

- 1 **Initialize** empty forest $F \leftarrow \emptyset$
- 2 **for** $t = 1$ **to** T **do**
- 3 Sample random subset X_t from X
- 4 Build isolation tree T_t on X_t
- 5 Add T_t to F
- 6 **return** F
- 7 **for each** $x_i \in X$ **do**
- 8 Compute average path length $h(x_i)$ across all trees
- 9 Calculate anomaly score $S(x_i)$ based on $h(x_i)$
- 10 **Sort** all instances x_i by $S(x_i)$ in descending order
- 11 **Calculate** threshold θ as the anomaly score of the instance at position $\lfloor c \cdot n \rfloor$
- 12 **for each** $x_i \in X$ **do**
- 13 **if** $S(x_i) < \theta$ **then**
- 14 Assign pseudo-label $y_i = 1$
- 15 **else**
- 16 Assign pseudo-label $y_i = 0$

Algorithm 2: Autoencoder for pseudo-labeling

Input: $X = \{x_1, x_2, \dots, x_n\}$ - Input dataset with n instances
Input: AE model = Encoder, Decoder
Input: θ_{error} - Threshold for reconstruction error
Output: Pseudo-labeled data with labels y_i

- 1 **for each** $x_i \in X$ **do**
- 2 **Encode** $h_i = f_{\text{encoder}}(x_i)$ - Map input to hidden representation
- 3 **Decode** $\hat{x}_i = f_{\text{decoder}}(h_i)$ - Reconstruct the input from hidden representation
- 4 **Calculate reconstruction error** $e_i = \|x_i - \hat{x}_i\|^2$
- 5 **for each** $x_i \in X$ **do**
- 6 **if** $e_i > \theta_{error}$ **then**
- 7 Assign pseudo-label: $y_i = 1$
- 8 **else**
- 9 Assign pseudo-label: $y_i = 0$

3.4 Model architectures

This subsection describes the LSTM, Transformer, and hybrid model architectures for anomaly detection, leveraging the pseudo-labels generated by the unsupervised anomaly detection models. The LSTM and Transformer models were selected for their ability to model sequential and long-range dependencies, with a hybrid model combining their strengths via stacking. The models were trained using sliding window sequences as input, with pseudo-labels from iForest and AE as target outputs.

3.4.1 LSTM model. LSTMs are well-suited for capturing long-term dependencies within sequential data, making them effective for anomaly detection in billing records. This stems from their use of memory cells and gating mechanisms, which mitigate the vanishing gradient problem found in traditional RNNs [5, 18, 23]. The model used in this study consists of two LSTM layers with 64 hidden units each, followed by a fully connected output layer. A single-layer variant was used for the original-label model on the declaration-level dataset, as it demonstrated better performance during training.

3.4.2 Transformer model. Transformers were chosen for their ability to capture long-range dependencies without relying on sequential processing. Their self-attention mechanism enables the model to determine the importance of each input element, which is useful for identifying subtle, temporal anomalies in billing records. This study adapted the encoder architecture from the Anomaly Transformer by Xu et al. [47], originally developed for unsupervised time series anomaly detection. The adapted model includes three encoder layers, each containing multi-head self-attention with eight attention heads, positional encoding, and a feedforward network with a hidden size of 512. Instead of reconstruction, a classification head consisting of a linear layer applied to the final timestep embedding was added. The Anomaly Transformer extends self-attention by modeling temporal dependencies via learned prior and series associations. The prior association uses a learnable Gaussian kernel to emphasize local dependencies, allowing the model to detect anomalies in nearby time windows. The series association captures broader patterns by learning attention weights across the full sequence, enabling the detection of long-span anomalies. The adapted Anomaly Transformer architecture is shown in Figure 2.

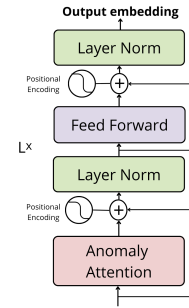


Figure 2: Adapted Anomaly Transformer architecture. The model employs Anomaly-Attention layers and feed-forward networks, each with residual connections and layer normalization. The reconstruction component is replaced with a classification head after the final encoder block.

3.4.3 Hybrid model. To combine the strengths of the LSTM and Transformer models, a stacking ensemble approach was used. Unlike bagging or boosting, which typically use homogeneous base learners and deterministic aggregation, stacking allows the integration of heterogeneous architectures. As a non-deterministic method, stacking combines predicted class labels from independently trained base models and uses them as input features for a meta-learner to

produce the final classification. By doing so, stacking can potentially minimize the prediction error, reduce noise, and explore the combined power of different models, as demonstrated by Cao et al. [8]. Logistic Regression (LR) was selected as the meta-learner due to its simplicity, robustness, and efficiency in low-dimensional spaces, as it only processes the base models' outputs. A recent study by Shafieian and Zulkernine [39] further supports this approach, showing that stacking outperforms bagging and boosting in detecting anomalies within complex network environments.

3.5 Experimental setup

A series of experiments evaluated the LSTM, Transformer, and hybrid models. All models were trained on both the original-label and their corresponding pseudo-labeled datasets, resulting in six variants. Unsupervised anomaly detection was performed locally, while model training and evaluation were run on the Snellius supercomputer¹. The hyperparameter settings for all models are provided in Appendix A.

3.5.1 Unsupervised anomaly detection. An 80/20 train-test split was applied before training the unsupervised models. With scarce ground-truth labels and a single fraud case unlikely to represent the full range of anomaly patterns, traditional evaluation metrics were not applicable. Instead, anomaly score distributions and label assignment behavior were analyzed. Both iForest and AE models were optimized using random search and executed multiple times to account for variability. The best performing configurations were selected based on mean absolute deviation for iForest and negative mean absolute error for the AE.

For iForest, the contamination threshold was set at 1.6% based on domain expertise. Instances exceeding this threshold received a pseudo-label of 1. The AE consisted of an encoder and decoder, each with two fully connected layers using ReLU activation. The encoder included two hidden layers, and the decoder mirrored this structure, ending with an output layer using Sigmoid activation. Early stopping was applied during training with a patience of eight epochs. Anomalies were identified using reconstruction error based on mean absolute error, applying the same 1.6% threshold used for iForest and guided by domain knowledge.

3.5.2 Baseline and hybrid models. LSTM and Transformer models served as baselines. All models used a 60/20/20 train-validation-test split, applied in chronological order to prevent temporal leakage. Validation sets were used for model tuning, hyperparameter optimization, and early stopping. Test sets were held out for final evaluation.

LSTM and Transformer models were implemented in PyTorch and trained separately on each of the six dataset variants. Both models used a weighted binary cross-entropy loss, with dataset-specific positive weights, and were optimized using Adam. Training ran up to 50 epochs, with early stopping based on validation loss. Classification thresholds were selected using the F1-score from the precision-recall curve or set to 0.5 if no optimum was found. To ensure reliable results, all models were run multiple times using the optimal threshold.

LSTM models used a dropout rate of 0.5 to reduce overfitting, except for the original-label declaration-level dataset, where dropout was not applicable. Early stopping was applied after seven epochs of stagnant validation loss, and a ReduceLRonPlateau scheduler reduced the learning rate by 0.5 after 5 epochs without improvement. Transformer models were trained without dropout but used a custom learning rate scheduler that halved the learning rate after each epoch to stabilize convergence. Early stopping was triggered after 10 epochs without improvement.

The hybrid model used LR to combine the label predictions from LSTM and Transformer models. For each dataset variant, predicted class labels from both models on validation and test sets were used as feature sets. LR was trained on validation features, with the two models' validation labels as the target. Class weights were set to 'balanced' to adjust for class imbalance.

3.6 Model interpretation and explainability

SHapley Additive exPlanations (SHAP) [27] was applied to improve the interpretability of complex deep learning models. Based on principles from game theory, SHAP assigns Shapley values to individual features, capturing their contribution to each prediction. This provides a clear understanding of the importance of input features in the decision-making process of deep learning models.

3.7 Performance evaluation metrics

To evaluate the performance of the hybrid and baseline models, precision, recall, and F1-score were used as the primary performance metrics. These metrics were calculated for each model across both original and pseudo-labeled datasets. Accuracy was included for completeness but interpreted with caution, as it can overestimate performance by favoring the majority class. For example, a naive classifier could achieve 99% accuracy simply by labeling all samples as non-anomalous. Precision measured the proportion of correctly classified anomalous instances, while recall measured the proportion of actual anomalous instances correctly identified by the classifier. The F1-score provided the harmonic mean of recall and precision. Additionally, McNemar's test [29] was applied to assess whether the difference in classification errors between two models trained on the same pseudo-labels was statistically significant.

4 RESULTS

This section evaluates the anomaly detection performance of the baseline and hybrid models on both the declaration- and operation-level datasets. The results demonstrate the effectiveness of the proposed models in handling highly imbalanced and skewed data.

4.1 Unsupervised anomaly detection

To address SQ1, the quality of the pseudo-labels generated by the iForest and AE models is assessed using t-SNE embeddings and density plots of anomaly scores and reconstruction errors. In both datasets, AE-based pseudo-labels show clearer separation between normal and anomalous instances, indicating stronger anomaly isolation. iForest performs comparatively well on the operation-level dataset, where anomalies are grouped more closely together.

¹<https://www.surf.nl/diensten/rekenen/snellius-de-nationale-supercomputer>

4.1.1 *T-SNE embeddings.* The operation-level dataset was sub-sampled to 50,000 instances due to computational limits. For the declaration-level dataset, the iForest t-SNE plot (Figure 3) shows scattered anomalies with limited separability. In contrast, the AE t-SNE plot (Figure 4) reveals clearer separation, with anomalies forming distinct localized clusters. On the operation-level dataset (Appendix B) both models show improved clustering. AE anomaly clusters appear near the lower edge of the embedding space, while iForest anomalies form clusters in the lower central region. This indicates that AE better captures the underlying structure of anomalies, making it possible to identify deviant patterns more effectively.

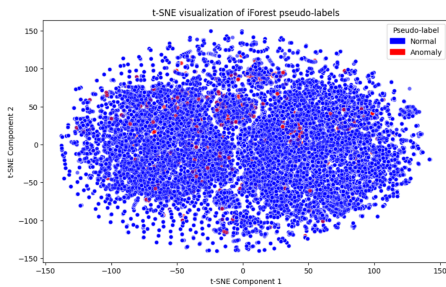


Figure 3: T-SNE plot of Isolation Forest pseudo-labels for the declaration-level dataset. Anomalous instances are scattered with limited separation from normal instances.

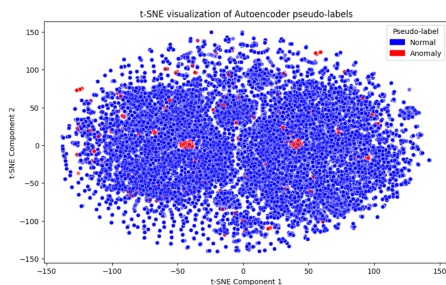


Figure 4: T-SNE plot of Autoencoder pseudo-labels for the declaration-level dataset. Anomalous instances form multiple localized clusters, indicating clearer separation.

4.1.2 *Anomaly distribution.* The density plots reveal the distribution of anomaly scores (iForest) and reconstruction errors (AE) by pseudo-labels. For the declaration-level dataset, the iForest distribution (Figure 5) shows a clear separation, with normal instances peaking at 0.05 and anomalies at -0.025, with a threshold of -0.01. The operation-level plot (Appendix B) follows a similar pattern, with even clearer separation. For the AE model, the declaration-level errors (Figure 6) show normal instances peaking at 0.05 and anomalies peaking at 0.10, with a threshold of 0.08. The operation-level distribution (Appendix B) is more spread out. However, normal instances form two peaks around 0.10 and 0.11, with limited overlap, indicating that most normal instances fall within this range.

Across both datasets, iForest anomaly scores are left-skewed, reflecting that anomalies tend to receive lower scores. In contrast, AE reconstruction errors are right-skewed, indicating that anomalies typically have larger reconstruction errors compared to normal instances. These patterns align with expectations for imbalanced data, where rare instances appear in the distribution tails.

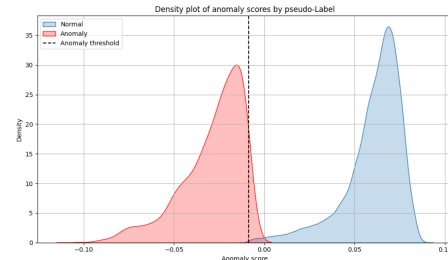


Figure 5: Density plot of Isolation Forest anomaly scores for the declaration-level dataset. Normal instances peak around 0.05, while anomalies peak near -0.025, showing clear separation with a decision threshold at -0.01.

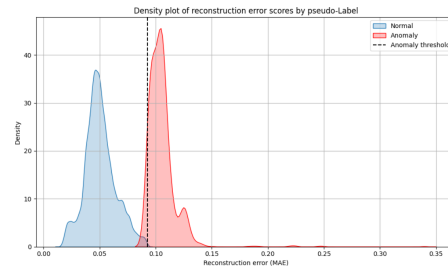


Figure 6: Density plot of Autoencoder reconstruction errors for the declaration-level dataset. Normal instances peak at 0.05, while anomalies peak around 0.10. The threshold at 0.08 indicates strong separability between the two groups.

To assess the alignment between iForest and AE, their pseudo-label agreement was examined. In both datasets, pseudo-label agreement exceeds 97% for normal instances (label 0). In contrast, only a small fraction of both datasets are consistently labeled as anomalies (label 1). Approximately 2.7% of instances show disagreement, where one model labels an instance as anomalous while the other does not. This limited overlap in positive labels highlights fundamental differences in how the models define anomalies, consistent with the patterns observed in the t-SNE embeddings. Full label agreement statistics are provided in Appendix B.

To better understand the identified anomalies, the top ten highest-scoring instances were selected for each model, allowing manageable analysis while capturing key model differences. In the declaration-level dataset, one client appears three times in the iForest top ten and five times in the AE top ten, with three declared files flagged by both. In the operation-level dataset, one client appears six times in the iForest top ten, with each instance corresponding to the same declaration file. AE identifies this same client twice,

but for different files, and highlights another client six times across three different declaration files. These patterns suggest that iForest focuses on repeated structural anomalies within a single context, while AE tends to identify a wider spread of anomalies across different files or entities. This implies that iForest may be better suited for detecting recurring, structural anomalies, while AE may be more effective at uncovering diverse and context-specific anomalies. Feature statistics are included in Appendix B.

4.2 Model performance

In relation to SQ2, this subsection compares the anomaly detection performance of the baseline models and hybrid models trained on the pseudo-labeled and original-label data. Model performance is evaluated using accuracy, precision, recall, and F1-score. Statistical differences in classification errors are assessed using McNemar’s test. The results from the test set, reflecting model generalization, are discussed. Table 1 and Table 2 present the results for the declaration-level and operation-level datasets. Validation set results are provided in Appendix C for completeness.

4.2.1 McNemar’s test. McNemar’s test reveals that the differences in classification errors between the LSTM and Transformer models are statistically significant under the same pseudo-labeling conditions. This holds for both the declaration-level and operation-level datasets, using iForest and AE pseudo-labels, across validation and test sets ($p < 0.05$). This suggests that model architecture has a substantial impact on anomaly detection behavior, even when trained on identical pseudo-labels. Detailed contingency tables are included in Appendix C.

4.2.2 iForest-based models. Among the baseline models, iForest-based models perform consistently well on both datasets. On the declaration-level dataset, the iForest LSTM achieves the highest scores across all metrics. The iForest Transformer performs reasonably but shows lower recall, suggesting a tendency to miss true anomalies. The hybrid iForest-based model demonstrates moderate improvement over the Transformer, though the iForest LSTM remains the strongest performer overall. On the operation-level dataset, the iForest LSTM again outperforms all models, achieving the best results on both validation and test sets. In contrast, the iForest Transformer shows a significant drop in test performance relative to its validation results, reflecting poor generalization. Except for the iForest LSTM, all models show substantial drops in generalization, indicating overfitting to the training data. The hybrid variant achieves the highest recall but still lags behind the iForest LSTM in overall accuracy, precision, and F1-score.

4.2.3 AE-based models. AE-based models show strong performance on the declaration-level dataset but struggle to generalize to more complex data. Both the AE LSTM and AE Transformer perform reasonably well, though with lower recall. Notably, the AE LSTM achieves higher precision and recall on the test set than on the validation set. This can be the result of a higher anomaly proportion in the test set compared to the validation set, creating more opportunities for the model to correctly identify these anomalies. The hybrid AE-based model outperforms its baselines in recall and F1-score but with a slight reduction in precision. In contrast, on the operation-level dataset, AE-based models perform poorly. Both

the AE Transformer and AE LSTM show severe drops in performance, with results below random guessing. While the AE LSTM performs moderately on the validation set, its test performance drops significantly, indicating overfitting. The hybrid variant also fails to improve performance, further demonstrating the difficulty AE-based models have in generalizing to more complex data.

4.2.4 Generalization and dataset complexity. A key insight in addressing SQ3 is the variation in model performance across datasets. While iForest-based models, particularly the iForest LSTM and its hybrid variant, consistently outperform others, most models show notable performance drops on the operation-level setting. This suggests that the operation-level dataset may be too complex for the models to reliably distinguish anomalies and produce consistent results. Moreover, hybrid models tend to increase recall at the cost of precision. These patterns underscore the importance of selecting models based on the specific anomaly detection task and highlight the potential of hybrid models to balance sensitivity and generalization.

4.2.5 Original-label based models. Across both datasets, original-label models consistently fail to detect anomalies. All baseline and hybrid variants score zero across evaluation metrics. While some models show minor results on the validation sets, their overall performance remains poor. In several test splits, no labeled anomalies were present, preventing the models from distinguishing normal from anomalous instances. This consistent failure likely reflects extreme class imbalance, which leaves the models unable to learn meaningful patterns from the minority class. It suggests that model architecture alone is not sufficient without label enrichment, even when adopting deep learning models. These results confirm the limitations of using standard supervised learning techniques while dealing with highly imbalanced data. As noted by Benchaji et al. [6], traditional classifiers often fail to detect anomalies when normal instances dominate.

Table 1: Model performance on the declaration-level dataset based on test set metrics. iForest LSTM achieves the highest performance across all metrics. Models trained on original labels fail to detect anomalies.

Classifiers	Accuracy	Precision	Recall	F1
Baseline models				
AE Transformer	0.987	0.940	0.556	0.698
iForest Transformer	0.994	0.806	0.876	0.840
Original-label Transformer	0.000	0.000	0.000	0.000
AE LSTM	0.991	0.912	0.705	0.795
iForest LSTM	0.999	0.995	0.963	0.959
Original-label LSTM	0.520	0.000	0.000	0.000
Hybrid models				
Hybrid AE based	0.991	0.901	0.715	0.798
Hybrid iForest based	0.996	0.818	0.963	0.884
Hybrid original-label based	0.000	0.000	0.000	0.000

Table 2: Model performance on the operation-level dataset based on test set metrics. IForest LSTM achieves the best overall balance of precision and recall. The hybrid iForest-based model improves recall but with reduced precision. All original-label models fail to identify anomalies.

Classifiers	Accuracy	Precision	Recall	F1
Baseline models				
AE Transformer	0.997	0.216	0.099	0.136
iForest Transformer	0.977	0.183	0.298	0.226
Original-label Transformer	0.735	0.000	0.000	0.000
AE LSTM	0.995	0.150	0.310	0.202
iForest LSTM	0.996	0.918	0.699	0.794
Original-label LSTM	1.0	0.000	0.000	0.000
Hybrid models				
Hybrid AE based	0.995	0.148	0.310	0.200
Hybrid iForest based	0.976	0.279	0.744	0.406
Hybrid original-label based	1.0	0.000	0.000	0.000

4.3 SHAP

Figure 7 and Figure 8 present a SHAP-based interpretability analysis of the iForest LSTM model. As the best-performing model, it was selected for explainability evaluation. The SHAP bar plot shows that the payment term (PayT_6_t18) is the most important feature, indicating that earlier time step values strongly influence anomaly predictions. The SHAP summary plot reveals that both high and low feature values impact predictions, suggesting a context-dependent role. Other top features, such as EarlyP_t81 (early payments) and PayT_2_t99, show that lower feature values are associated with higher SHAP values, increasing the likelihood of the model predicting an anomaly. Features like hour_cos_t30 show low importance, indicating limited relevance of cyclical time. Additional SHAP plots for baseline models are included in Appendix D.

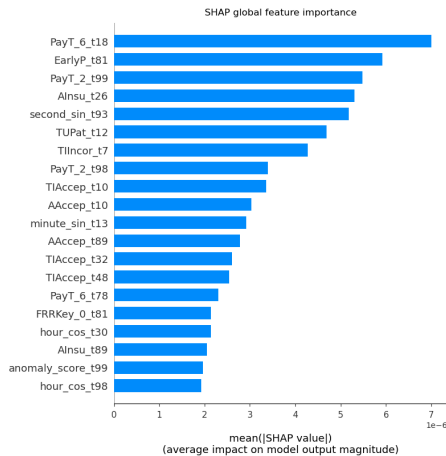


Figure 7: SHAP summary bar plot, demonstrating the top 20 most influential features in the iForest LSTM model. Features related to payment timing and opting for early payment dominate feature importance.

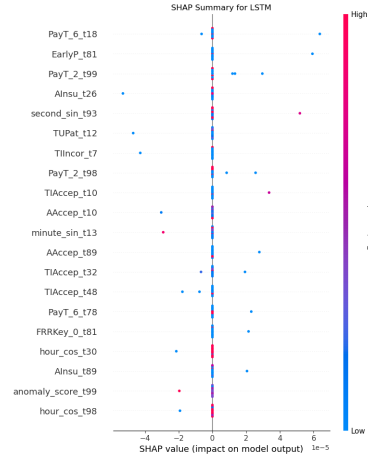


Figure 8: SHAP summary plot, demonstrating the distribution and direction of feature impact in the iForest LSTM model. High and low feature values influence anomaly predictions in a context-dependent manner.

5 DISCUSSION

This section reflects on the methods employed, evaluating their strengths and limitations, and outlines directions for future research. Moreover, ethical considerations are discussed, particularly the implications of applying deep learning in sensitive domains like mental healthcare billing. Lastly, it outlines opportunities for future research.

5.1 Analysis of findings

The iForest LSTM model achieved the highest performance across both datasets. This aligns with prior work by Benchaji et al. [6], who demonstrated that LSTMs are effective in capturing long-term dependencies in sequential financial data. The success of the iForest LSTM model in this study further supports the applicability of sequential deep learning models in the context of billing fraud. Transformer models, while promising in other anomaly detection domains [44, 47, 50], showed less stable performance in this study. This may be due to the complexity of tuning attention-based architectures and their sensitivity to noise and variation in the input features. McNemar’s test confirmed significant classification error differences between LSTM and Transformer models, even when trained on identical pseudo-labels. This highlights that the architecture choice, combined with the labeling strategy, has a substantial impact on prediction outcomes. Only the iForest-based hybrid model yielded more robust outputs, though not surpassing the iForest LSTM baseline. This contrasts with findings by Ileberi and Sun [18], who reported that hybrid architectures outperformed individual learners in credit card fraud detection. A possible explanation is their use of the European Credit Card Dataset from 2013. Given its age, the dataset may not reflect current fraud patterns or the complexity of domain-specific billing data, limiting the generalizability of their results. The complete failure of the original-label models to detect anomalies further confirms the findings of Kulatilleke [22], who emphasized the limitations of supervised learning under

extreme class imbalance. In contrast, the use of pseudo-labeling improved model performance, aligning with the findings of Al-Lahham et al. [2] and Im et al. [19], who showed that unsupervised labeling can be effective when labeled anomalies are limited or unavailable.

Although t-SNE visualizations showed greater separability for pseudo-labels generated by the AE, models trained on iForest pseudo-labels consistently performed better. AE pseudo-labels may retain noise and fail to effectively distinguish anomalies from normal instances. This highlights that visual interpretability does not always translate to practical utility. Future work could explore ensemble methods to combine the strengths of both approaches.

5.2 Limitations

While this study demonstrates promising results, several limitations must be acknowledged. First, the use of proprietary mental healthcare billing data limits reproducibility. Due to privacy and contractual restrictions, the datasets are not publicly available, which constrains replication of the findings. Moreover, since the datasets originate from a single healthcare declaration source and focus exclusively on mental healthcare, the model is influenced by specific billing practices, domain-specific policies, and fraud patterns. Applying it in other domains or contexts may therefore require retraining to accommodate different data characteristics.

A further consideration involves how the model’s output should be interpreted. Since the labeling process relies on unsupervised learning rather than confirmed fraud cases, some of the detected anomalies may represent unusual but legitimate billing behavior. This underscores the need for expert review to assess flagged anomalies. For instance, Ding et al. [13] proposed the ALARM framework, which integrates a human-in-the-loop approach into the anomaly detection pipeline by incorporating iterative expert review and explanation mechanisms. Adopting similar strategies in mental healthcare billing could help reduce false positives and ensure that automated detection remains aligned with domain expertise. Additionally, while SHAP offers partial insight into the models’ decision-making, it provides only a limited understanding of their underlying reasoning. As such, deploying these models in high-stakes environments should be approached with caution and transparency.

5.3 Ethical and practical considerations

The application of deep learning models for anomaly detection in mental healthcare billing raises ethical and practical considerations. While these models can flag potential fraud cases that might otherwise go unnoticed, the trade-off between precision and recall is crucial in this domain. Favoring high recall would mean detecting more possible fraud cases and may be prioritized over precision to minimize financial losses. However, this could lead to increased false positives, misclassifying legitimate billing and risking providers’ reputations. Since anomalies do not always indicate fraud, domain expertise is vital to interpret outputs and distinguish errors from real fraud cases. Moreover, the black-box nature of deep learning models requires a human-in-the-loop approach to ensure

transparency and accountability. Model outputs should prompt expert review, not automated decisions, and patient privacy should always be prioritized over the pursuit of performance metrics.

Another constraint relates to the computational demands of the models. Although hybrid models showed some performance gains, training deep learning models required significant resources and time. This could hinder adoption in settings without access to high-performance computing infrastructures. Transformers, in particular, pose scalability challenges due to their quadratic memory complexity. Practical deployment may require model compression, optimization, or less computationally expensive architectures to ensure feasibility.

5.4 Future work

Future research could assess whether the hybrid model generalizes to other domains, such as dentistry or insurance fraud. This would clarify whether the performance gains are generalizable or specific to mental healthcare data. Another key direction is improving model performance on complex data like the operation-level dataset. In this study, performance dropped significantly, especially for the Transformer models. Potential directions include exploring methods to handle this complexity or more targeted feature engineering informed by domain knowledge. While this study implemented a two-layer LSTM, other recurrent configurations were not explored. Future research could evaluate different architectures, such as bidirectional LSTMs, as well as variations in hidden units and sequence lengths, to assess their effect on anomaly performance. Furthermore, future work should consider the trade-offs between model complexity and performance, as this study demonstrated that increased complexity does not always yield better results. Finally, while unsupervised pseudo-labeling improved results, it could be interesting to experiment with different synthetic anomaly generation techniques to further enhance pseudo-labeling quality.

6 CONCLUSION

This study addressed the challenge of anomaly detection in mental healthcare billing, a domain marked by class imbalance and fraud risks. It investigated whether a hybrid LSTM-Transformer model could enhance anomaly detection in imbalanced billing data and evaluated the role of pseudo-labeling in improving model performance. The iForest LSTM model outperformed both baseline and hybrid models, indicating that simpler sequential models are more effective in this setting. The hybrid iForest-based model, though not surpassing iForest LSTM, demonstrated promising results by improving the standalone Transformer, AE, and supervised models. Pseudo-labeling, particularly with iForest, significantly enhanced model performance over training on original labels, confirming its value in settings with extreme label scarcity.

This research contributes to the field of unsupervised anomaly detection by validating the effectiveness of pseudo-labeling in the mental healthcare billing domain. It highlights the trade-offs between model complexity and performance, suggesting that simpler architectures may be more suitable for practical deployment. Future work could focus on model variants and synthetic anomaly generation to address data imbalance and improve pseudo-label quality, while also evaluating generalizability across domains.

REFERENCES

- [1] Abhaya Abhaya and Bidyut Kr. Patra. 2023. An efficient method for autoencoder based outlier detection. *Expert Systems with Applications* 213 (3 2023). doi:10.1016/j.eswa.2022.118904
- [2] Anas Al-Lahham, Nurbek Tastan, Zaigham Zaheer, and Karthik Nandakumar. 2023. A Coarse-to-Fine Pseudo-Labeling (C2FPL) Framework for Unsupervised Video Anomaly Detection. *arXiv (Cornell University)* (1 2023). doi:10.48550/arxiv.2310.17650
- [3] Algemene Rekenkamer. 2022. Een zorgelijk gebrek aan daadkracht: Onderzoek naar de effectiviteit van zorgfraudebestrijding. <https://www.rekenkamer.nl/publicaties/rapporten/2022/04/14/een-zorg-gebrek-aan-daadkracht>
- [4] Matin N. Ashtiani and Bijan Raahemi. 2022. Intelligent Fraud Detection in Financial Statements Using Machine Learning and Data Mining: A Systematic Literature Review. *IEEE Access* 10 (2022), 72504–72525. doi:10.1109/ACCESS.2021.3096799
- [5] Ari Yair Barrera-Animas, Lukumon O. Oyedele, Muhammad Bilal, Taofeek Dolapo Akinosho, Juan Manuel Davila Delgado, and Lukman Adewale Akanbi. 2022. Rain-fall prediction: A comparative analysis of modern machine learning algorithms for time-series forecasting. *Machine Learning with Applications* 7 (2022), 100204. doi:10.1016/j.mlwa.2021.100204
- [6] Ibtissam Benchaji, Samira Douzi, and Bouabid El Ouahidi. 2021. Credit Card Fraud Detection Model Based on LSTM Recurrent Neural Networks. *Journal of Advances in Information Technology* 12, 2 (1 2021), 113–118. doi:10.12720/jait.12.2.113-118
- [7] Kaidi Cao, Colin Wei, Adrien Gaidon, Nikos Arachiga, and Tengyu Ma. 2019. Learning Imbalanced Datasets with Label-Distribution-Aware Margin Loss. *arXiv (Cornell University)* (1 2019).
- [8] Kangjie Cao, Ting Zhang, and Jueqiao Huang. 2024. Advanced hybrid LSTM-transformer architecture for real-time multi-task prediction in engineering systems. *Scientific Reports* 14, 1 (2 2024). doi:10.1038/s41598-024-55483-x
- [9] Agniv Chatterjee, S. Sahand Mohammadi Ziabari, and Amr Elsherbini. 2023. *Payments Fraud Detection using ML methods: Exploring Performance, Ethical and Real-World Considerations in Machine Learning-based Fraud Detection for Secure Payments*. Technical Report. University of Amsterdam & Deloitte. Retrieved via ResearchGate.
- [10] Patricia Craja, Alisa Kim, and Stefan Lessmann. 2020. Deep learning for detecting financial statement fraud. *Decision Support Systems* 139 (10 2020), 113421. doi:10.1016/j.dss.2020.113421
- [11] Andrea Dal Pozzolo, Giacomo Boracchi, Olivier Caelen, Cesare Alippi, and Gianluca Bontempi. 2018. Credit Card Fraud Detection: A Realistic Modeling and a Novel Learning Strategy. *IEEE Transactions on Neural Networks and Learning Systems* 29, 8 (2018), 3784–3797. doi:10.1109/TNNLS.2017.2736643
- [12] Rohan Deshamudre, S. Sahand Mohammadi Ziabari, and Marc van Houten. 2023. Enhancing AI Adoption in Healthcare: A Data Strategy for Improved Heart Disease Prediction Accuracy through Deep Learning Techniques. In *Proceedings of the ACM Symposium on Applied Computing*. doi:10.1007/978-3-031-48316-5_2
- [13] Xueying Ding, Nikita Seleznev, Senthil Kumar, C. Bayan Bruss, and Leman Akoglu. 2023. From Explanation to Action: An End-to-End Human-in-the-loop Framework for Anomaly Reasoning and Management. *arXiv (Cornell University)* (1 2023). doi:10.48550/arxiv.2304.03368
- [14] Fabian Dubourvieux, Romaric Audigier, Angélique Loesch, Samia Ainouz, and Stéphane Canu. 2022. A formal approach to good practices in Pseudo-Labeling for Unsupervised Domain Adaptive Re-Identification. *Computer Vision and Image Understanding* 223 (8 2022), 103527. doi:10.1016/j.cviu.2022.103527
- [15] Shawni Dutta and Samir Kuma Bandyopadhyay. 2020. Detection of Fraud Transactions Using Recurrent Neural Network during COVID-19. *Journal of Advanced Research in Medical Science and Technology* 07, 03 (10 2020), 16–21. doi:10.24321/2394.6539.202012
- [16] Zain Hamid, Fatima Khalique, Saba Mahmood, Ali Daud, Amal Bukhari, and Bader Alshemaimri. 2024. Healthcare insurance fraud detection using data mining. *BMC Medical Informatics and Decision Making* 24, 1 (4 2024). doi:10.1186/s12911-024-02512-4
- [17] Lu Han, Han-Jia Ye, and De-Chuan Zhan. 2023. On Pseudo-Labeling for Class-Mismatch Semi-Supervised Learning. *arXiv (Cornell University)* (1 2023). doi:10.48550/arxiv.2301.06010
- [18] Emmanuel Ileberi and Yanxia Sun. 2024. A Hybrid Deep Learning Ensemble Model for Credit Card Fraud Detection. *IEEE Access* 12 (2024), 175829–175838. doi:10.1109/ACCESS.2024.3502542
- [19] Jiin Im, Yongho Son, and Je Hyeong Hong. 2024. FUN-AD: Fully Unsupervised Learning for Anomaly Detection with Noisy Training Data. *arXiv (Cornell University)* (11 2024). doi:10.48550/arxiv.2411.16110
- [20] Yashvi Jain, Namrata Tiwari, Shripriya Dubey, and Sarika Jain. 2019. A comparative analysis of various credit card fraud detection techniques. *International Journal of Recent Technology and Engineering* 7, 5 (2019), 402–407.
- [21] Eunji Kim, Jehyuk Lee, Hunsik Shin, Hoseong Yang, Sungzoon Cho, Seung-Kwan Nam, Youngmi Song, Jeong-A Yoon, and Jong-Il Kim. 2019. Champion-challenger analysis for credit card fraud detection: Hybrid ensemble and deep learning. *Expert Systems with Applications* 128 (3 2019), 214–224. doi:10.1016/j.eswa.2019.03.042
- [22] Gayan K. Kulatilake. 2022. Challenges and Complexities in Machine Learning based Credit Card Fraud Detection. *arXiv (Cornell University)* (1 2022). doi:10.48550/arxiv.2208.10943
- [23] Deepak Kumar, Anshuman Singh, Pijush Samui, and Rishi Kumar Jha. 2019. Forecasting monthly precipitation using sequential modelling. *Hydrological Sciences Journal* 64, 6 (3 2019), 690–700. doi:10.1080/02626667.2019.1595624
- [24] Prateek Kumar Bansal, Divya Nimma, Nripendra Narayan Das, BVN Prasad Paruchuri, Harishchander Anandaram, and M. Karthik. 2024. Boosting Anomaly Detection in Financial Transactions: Leveraging Deep Learning with Isolation Forest for Enhanced Accuracy. (2024), 1–6. doi:10.1109/ICAIQSA64000.2024.10882180
- [25] Aodong Li, Chen Qiu, Padhraic Smyth, Marius Kloft, Stephan Mandt, and Maja Rudolph. 2023. Deep Anomaly Detection under Labeling Budget Constraints. *arXiv (Cornell University)* (1 2023). doi:10.48550/arxiv.2302.07832
- [26] Dong Liang, Jun Wang, Xiaoyu Gao, Jiahui Wang, Xiaoyong Zhao, and Lei Wang. 2022. Self-supervised Pretraining Isolated Forest for Outlier Detection. *2022 International Conference on Big Data, Information and Computer Network (BDICN)*, 306–310. doi:10.1109/BDICN55575.2022.00065
- [27] Scott Lundberg and Su-In Lee. 2017. A Unified Approach to Interpreting Model Predictions. *arXiv (Cornell University)* (5 2017). doi:10.48550/arxiv.1705.07874
- [28] Ahmed Marcouch and Marco van der Wel. 2023. Fenomeenanalyse Criminele zzz'ers in de zorg Arnhem - iBabs Publieksportaal. <https://arnhem.bestuurlijkeinformatie.nl/Reports/Item/4b3941ee-d0df-4160-bc1c-13ef09c160dd>
- [29] Quinn McNemar. 1947. Note on the sampling error of the difference between correlated proportions or percentages. *Psychometrika* 12, 2 (6 1947), 153–157. doi:10.1007/bf02295996
- [30] Ibomoye Dolor Mienye and Nibert Jere. 2024. Deep Learning for Credit Card Fraud Detection: A review of Algorithms, Challenges, and Solutions. *IEEE Access* 12 (1 2024), 96893–96910. doi:10.1109/access.2024.3426955
- [31] Soroor Motie and Bijan Raahemi. 2024. Financial fraud detection using graph neural networks: A systematic review. *Expert Systems with Applications* 240 (4 2024), 122156. doi:10.1016/j.eswa.2023.122156
- [32] Ali Vafaee Najari, Leili Alizamani, Marziye Zarqi, and Elaheh Hooshmand. 2025. A global scoping review on the patterns of medical fraud and abuse: integrating data-driven detection, prevention, and legal responses. *Archives of Public Health* 83, 1 (2 2025). doi:10.1186/s13690-025-01512-8
- [33] Jamal Abdul Nasir, Osama Subhani Khan, and Iraklis Varlamis. 2021. Fake news detection: A hybrid CNN-RNN based deep learning approach. *International Journal of Information Management Data Insights* 1 (1 2021), 100007. doi:10.1016/j.jjime.2020.100007
- [34] Pradheepan Raghavan and Neamat El Gayar. 2019. Fraud Detection using Machine Learning and Deep Learning. *2019 International Conference on Computational Intelligence and Knowledge Economy (ICCICE)*, 334–339. doi:10.1109/iccice47802.2019.9004231
- [35] Samad Riaz, Amna Saghir, Muhammad Junaid Khan, Hassan Khan, Hamid Saeed Khan, and M. Jaleed Khan. 2024. TransLSTM: A hybrid LSTM-Transformer model for fine-grained suggestion mining. *Natural Language Processing Journal* 8 (7 2024), 100089. doi:10.1016/j.nlp.2024.100089
- [36] J Femila Roseline, GBSR Naidu, V. Samuthira Pandi, S Alamelu Alias Rajasree, and Dr. N. Mageswari. 2022. Autonomous credit card fraud detection using machine learning approach. *Computers & Electrical Engineering* 102 (6 2022), 108132. doi:10.1016/j.compeleceng.2022.108132
- [37] Ruttala Sailusha, V. Gnaneswar, R. Ramesh, and G. Ramakoteswara Rao. 2020. Credit Card Fraud Detection Using Machine Learning. *2020 4th International Conference on Intelligent Computing and Control Systems (ICICCS)*, 1264–1270. doi:10.1109/ICICCS48265.2020.9121114
- [38] Thomas Schranz, Gerald Schweiger, Siegfried Pabst, and Franz Wotawa. 2020. *Machine Learning for Water Supply Supervision*. Springer International Publishing, 238–249 pages. doi:10.1007/978-3-030-55789-8_21
- [39] Saeed Shafeian and Mohammad Zulkernine. 2022. Multi-layer stacking ensemble learners for low footprint network intrusion detection. *Complex & Intelligent Systems* 9, 4 (7 2022), 3787–3799. doi:10.1007/s40747-022-00809-3
- [40] Feng Shen, Xingchao Zhao, Gang Kou, and Fawaz E. Alsaadi. 2021. A new deep learning ensemble credit risk evaluation model with an improved synthetic minority oversampling technique. *Applied Soft Computing* 98 (1 2021), 106852. doi:10.1016/j.asoc.2020.106852
- [41] Margot Smolenaars and Judith Spanjers. 2024. Klokkenluiders: grote jeugd-ggz-instelling fraudeert met zorggeld. (11 2024). <https://www.ftm.nl/artikelen/declaraties-jeugd-zorg-karakter-zorgfraude>
- [42] Khushboo Taneja, Jyoti Vashishtha, and Saroj Ratnoo. 2025. Fraud-BERT: transformer based context aware online recruitment fraud detection. *Discover Computing* 28 (2 2025). doi:10.1007/s10791-025-09502-8
- [43] Yuxuan Tang and Zhanjun Liu. 2024. A Credit Card Fraud Detection Algorithm Based on SDT and Federated Learning. *IEEE Access* 12 (2024), 182547–182560. doi:10.1109/ACCESS.2024.3491175

- [44] Yuxuan Tang and Zhanjun Liu. 2024. A Distributed Knowledge Distillation Framework for Financial Fraud Detection Based on Transformer. *IEEE Access* 12 (2024), 62899–62911. doi:10.1109/ACCESS.2024.3387841
- [45] Sandra Wilfling. 2023. Augmenting data-driven models for energy systems through feature engineering: A Python framework for feature engineering. *arXiv (Cornell University)* (1 2023). doi:10.48550/arxiv.2301.01720
- [46] Hongzuo Xu, Guansong Pang, Yijie Wang, and Yongjun Wang. 2023. Deep Isolation Forest for Anomaly Detection. *IEEE Transactions on Knowledge and Data Engineering* 35, 12 (4 2023), 12591–12604. doi:10.1109/tkde.2023.3270293
- [47] Jiehui Xu, Haixu Wu, Jianmin Wang, and Mingsheng Long. 2022. Anomaly Transformer: Time Series Anomaly Detection with Association Discrepancy. *arXiv (Cornell University)* (1 2022). doi:10.48550/arxiv.2110.02642
- [48] Jun Yang, Jingbin Qu, Qiang Mi, and Qing Li. 2020. A CNN-LSTM model for tailings dam risk prediction. *IEEE Access* 8 (11 2020), 206491–206502. doi:10.1109/access.2020.3037935
- [49] Jinsung Yoon, Kihyuk Sohn, Chun-Liang Li, Sercan O. Arik, and Tomas Pfister. 2022. SPADE: Semi-supervised Anomaly Detection under Distribution Mismatch. *arXiv (Cornell University)* (1 2022). doi:10.48550/arxiv.2212.00173
- [50] Chang Yu, Yongshun Xu, Jin Cao, Ye Zhang, Yinxin Jin, and Mengran Zhu. 2024. Credit card fraud detection using Advanced Transformer model. *arXiv (Cornell University)* (6 2024). doi:10.48550/arxiv.2406.03733
- [51] Weilian Zhou, Sei-Ichiro Kamata, Haipeng Wang, and Xi Xue. 2023. Multiscanning-Based RNN-Transformer for Hyperspectral Image Classification. *IEEE Transactions on Geoscience and Remote Sensing* 61 (2023), 1–19. doi:10.1109/TGRS.2023.3277014

Appendices

A HYPERPARAMETERS

For the sake of reproducibility, the tested and final hyperparameter settings for all models, including the unsupervised anomaly detection, are reported below. The tables are separated by model type and dataset-level. Given the computational costs of the LSTM and Transformer models, exhaustive methods such as grid search or random search were not feasible. Instead, hyperparameters, such as the learning rate, batch size, and patience, were adjusted based on performance trends during validation.

Table 3: Final optimized hyperparameters for Isolation Forest and Autoencoder models.

Isolation Forest	Declaration-level	Operation-level
Number of estimators	50	50
Max sample size	0.90	0.90
Max feature proportion	0.10	0.10
Bootstrapping	False	False
Contamination threshold (θ)	0.016	0.016
Autoencoder	Declaration-level	Operation-level
Optimizer	Adam	RMSprop
Learning rate	0.01	0.01
Hidden layer 1 neurons	32	16
Hidden layer 2 neurons	10	8
Activation (hidden layers)	ReLU	ReLU
Activation (output layer)	Sigmoid	Sigmoid
Early stopping patience	8 epochs	8 epochs
Total training epochs	28	18
Anomaly threshold (percentile)	98.4%	98.4%

Table 4: Hyperparameter grid for Isolation Forest.

Hyperparameter	Value
Number of estimators	[50, 100, 150, 200, 300]
Max sample size	['auto', 0.1, 0.3, 0.5, 0.7, 0.9]
Max feature proportion	[0.1, 0.3, 0.5, 0.7, 1.0]
Bootstrapping	[True, False]

Table 5: Hyperparameter grid for Autoencoder.

Hyperparameter	Value
Hidden layer 1 neurons	[16, 32]
Hidden layer 2 neurons	[8, 10]
Learning rate	[0.001, 0.01, 0.005, 0.05]
Optimizer	['adam', 'rmsprop', 'sgd']

Table 6: Randomized search settings for Isolation Forest.

Hyperparameter	Value
Number of iterations	10
Scoring	mean absolute deviation
cv	3-fold
Verbose	2
Random state	42

Table 7: Randomized search settings for Autoencoder.

Hyperparameter	Value
Epochs	50
Batch size	32
Callbacks	early stopping
Verbose	1

Table 8: LSTM hyperparameters and training outcomes for the declaration-level dataset.

Hyperparameter	Autoencoder	Isolation Forest	Original-label
Window size	100	100	100
Batch size	64	64	64
Positive weight	30	30	10
Weight decay	0.001	0.001	0.001
Learning rate	0.005	0.005	0.005
Patience	7	7	7
Epochs run	13	50	19
Optimal used threshold	0.875	0.936	0.0003
Validation loss	0.250	0.170	1.976
Test loss	0.331	0.181	0.0003

Table 9: LSTM hyperparameters and training outcomes for the operation-level dataset.

Hyperparameter	Autoencoder	Isolation Forest	Original-label
Window size	50	50	100
Batch size	64	64	64
Positive weight	30	30	10
Weight decay	0.001	0.001	0.001
Learning rate	0.0005	0.0005	0.0005
Patience	7	7	7
Epochs run	17	43	8
Optimal used threshold	0.296	0.901	0.002
Validation loss	0.057	0.042	0.079
Test loss	0.202	0.063	0.031

Table 10: Transformer hyperparameters and training outcomes for the declaration-level dataset.

Hyperparameter	Autoencoder	Isolation Forest	Original-label
Window size	100	100	100
Batch size	64	64	64
Positive weight	40	40	20
Activation function	Gelu	Gelu	Gelu
Learning rate	0.0001	0.0001	0.0001
Patience	5	5	10
Epochs run	14	11	11
Optimal used threshold	0.989	0.990	0.000
Validation loss	0.350	0.062	6.402
Test loss	0.317	0.060	0.000

Table 11: Transformer hyperparameters and training outcomes for the operation-level dataset.

Hyperparameter	Autoencoder	Isolation Forest	Original-label
Window size	50	50	100
Batch size	64	64	64
Positive weight	20	20	10
Activation function	Gelu	Gelu	Gelu
Learning rate	0.0001	0.0001	0.0005
Patience	10	10	10
Epochs run	21	25	18
Optimal used threshold	0.749	0.894	0.000
Validation loss	0.059	0.139	0.036
Test loss	0.180	0.362	0.006

B UNSUPERVISED ANOMALY DETECTION

Table 12: Pseudo-label agreement between Isolation Forest and Autoencoder models for the declaration-level and operation-level datasets. Label 0 indicates normal instances, and label 1 indicates anomalous instances.

Label combination	Count	Percentage
Declaration-level dataset		
Both label 1	184	0.26%
Both label 0	69,100	97.06%
iForest 1 and AE 0	956	1.34%
iForest 0 and AE 1	956	1.34%
Total	71,196	100%
Operation-level dataset		
Both label 1	4,581	0.29%
Both label 0	1,543,664	97.09%
iForest 1 and AE 0	20,859	1.31%
iForest 0 and AE 1	20,847	1.31%
Total	1,589,951	100%

Table 13: Summary statistics for selected features among the top 10 anomalies for the declaration-level dataset.

Model	Feature	Mean	Std	Min	Max
Isolation Forest	Anomaly score	-8.80e-2	6.35e-3	-1.02e-1	-8.13e-2
	AAccep	2.97e8	3.93e8	0.00	9.00e8
	ASup	3.01e8	3.91e8	6.20e6	9.02e8
	TOAccep	3.11e6	4.32e6	0.00	9.75e6
	TOStop	3.50e4	3.86e4	1.70e3	1.28e5
	AInsu	1.79e4	3.72e4	0.00	1.06e5
Autoencoder	Recon error	2.21e-1	5.15e-2	1.50e-1	3.40e-1
	AAccep	6.50e8	6.40e8	0.00	1.88e9
	ASup	6.79e8	6.05e8	2.72e3	1.88e9
	TOAccep	6.25e6	6.13e6	0.00	1.84e7
	TOStop	4.92e5	7.88e5	0.00	1.64e6
	AInsu	0.00	0.00	0.00	0.00

Table 14: Summary statistics for selected features among the top 10 anomalies for the operation-level dataset.

Model	Feature	Mean	Std	Min	Max
Isolation Forest	Anomaly score	-6.25e-2	8.04e-4	-6.35e-2	-6.13e-2
	AAccep	0.00	0.00	0.00	0.00
	ASup	1.85e4	1.53e4	5.00	3.03e4
	TOAccep	0.00	0.00	0.00	0.00
	TOSTop	1.07e2	8.75e1	1.00	1.75e2
	AInsu	0.00	0.00	0.00	0.00
Autoencoder	Recon error	1.13e-1	2.37e-3	1.10e-1	1.16e-1
	AAccep	8.33e6	6.45e6	0.00	1.41e7
	ASup	8.60e6	6.67e6	3.17e3	1.44e7
	TOAccep	5.26e4	4.17e4	0.00	9.45e4
	TOSTop	2.37e3	2.10e3	1.60e1	4.44e3
	AInsu	7.33e4	6.33e4	0.00	1.27e5

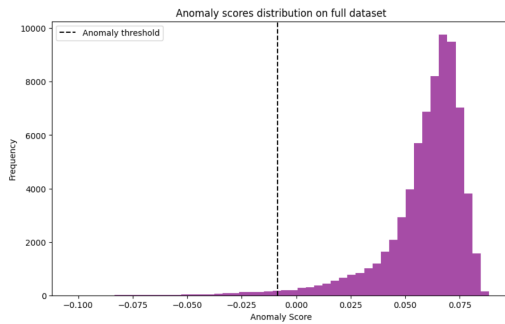


Figure 9: Anomaly score distribution of Isolation Forest for the declaration-level dataset.

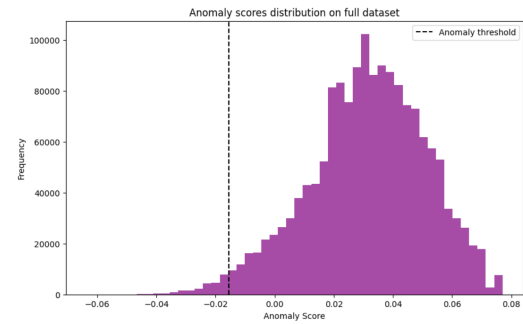


Figure 10: Anomaly score distribution of Isolation Forest for the operation-level dataset.

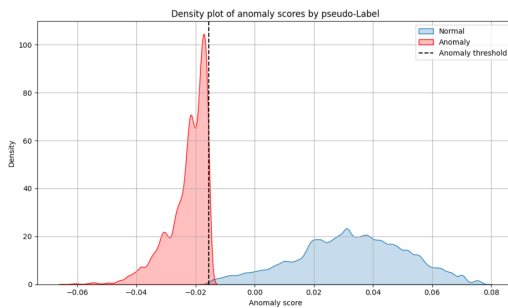


Figure 11: Density plot of Isolation Forest anomaly scores for the operation-level dataset.

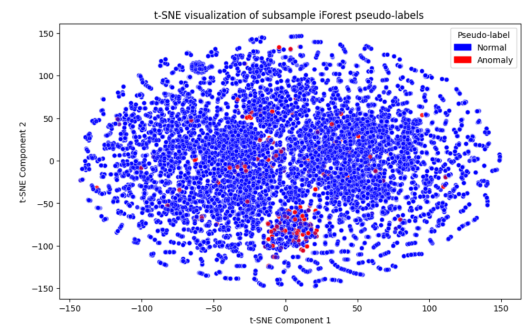


Figure 12: T-SNE plot of Isolation Forest pseudo-labels for the operation-level dataset.

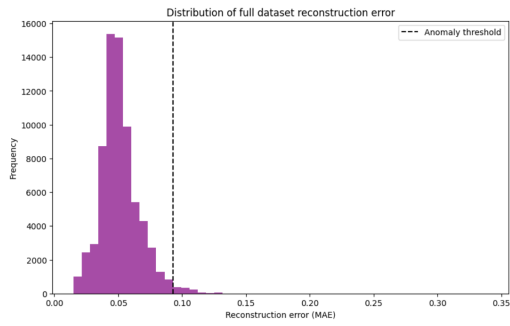


Figure 13: Reconstruction error distribution of Autoencoder for the declaration-level dataset.

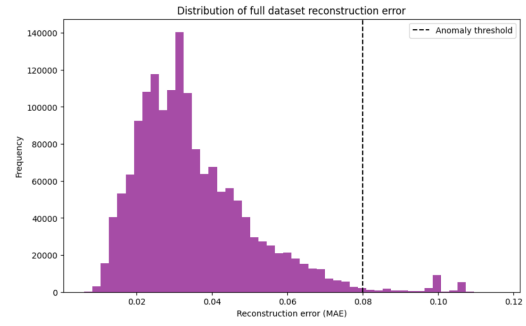


Figure 14: Reconstruction error distribution of Autoencoder for the operation-level dataset.

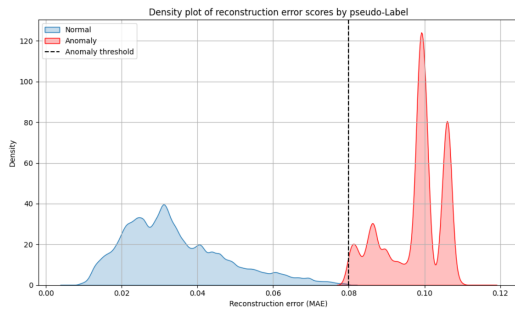


Figure 15: Density plot of Autoencoder reconstruction errors for the operation-level dataset.

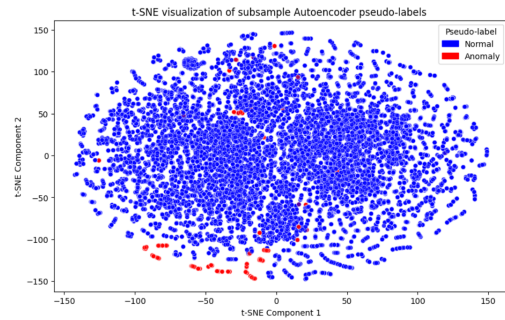


Figure 16: T-SNE plot of Autoencoder pseudo-labels for the operation-level dataset.

C MODEL PERFORMANCE

Table 15: McNemar’s test results for detecting significant differences in classification errors between LSTM and Transformer models on the test set.

Pseudo-label model	Statistic	P-value	Significant
Declaration-level dataset			
Autoencoder	21.25	0.00	Yes
Isolation Forest	57.14	0.00	Yes
Operation-level dataset			
Autoencoder	38.40	0.00	Yes
Isolation Forest	41.40	0.00	Yes

Table 16: McNemar’s test results for detecting significant differences in classification errors between LSTM and Transformer models on the validation set.

Pseudo-label model	Statistic	P-value	Significant
Declaration-level dataset			
Autoencoder	38.40	0.00	Yes
Isolation Forest	41.40	0.00	Yes
Operation-level dataset			
Autoencoder	121.18	0.00	Yes
Isolation Forest	5187.17	0.00	Yes

Table 17: Overview of model performance on the declaration-level dataset, based on evaluation metrics computed on the validation set.

Classifiers	Accuracy	Precision	Recall	F1-score
Baseline models				
AE Transformer	0.993	0.802	0.478	0.599
iForest Transformer	0.995	0.868	0.865	0.867
Original-label Transformer	0.995	0.219	0.315	0.258
AE LSTM	0.988	0.462	0.565	0.508
iForest LSTM	0.999	0.960	0.980	0.970
Original-label LSTM	0.634	0.043	0.656	0.081

Table 18: Overview of model performance on the operation-level dataset, based on evaluation metrics computed on the validation set.

Classifiers	Accuracy	Precision	Recall	F1-score
Baseline models				
AE Transformer	0.998	0.348	0.846	0.494
iForest Transformer	0.984	0.396	0.661	0.495
Original-label Transformer	0.999	0.000	0.000	0.000
AE LSTM	0.998	0.427	0.867	0.572
iForest LSTM	0.997	0.881	0.878	0.879
Original-label LSTM	0.997	0.056	0.295	0.094

D SHAP EXPLANATION

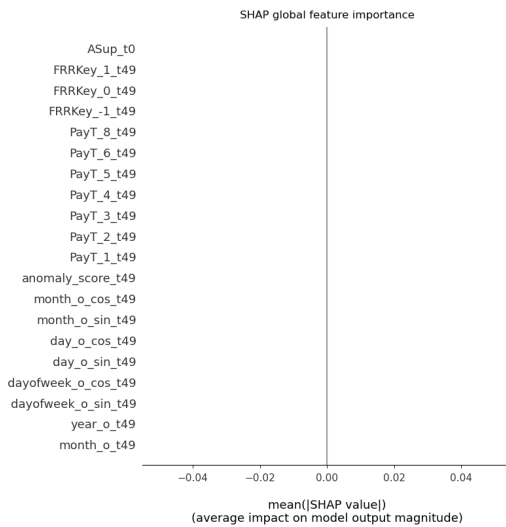


Figure 17: SHAP summary bar plot for Isolation Forest LSTM for the operation-level dataset.

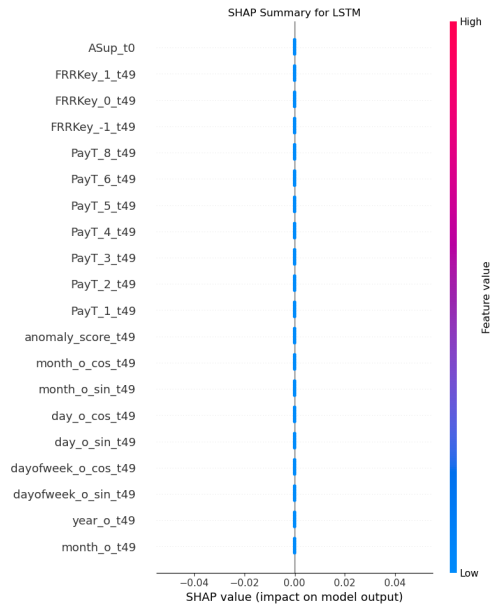


Figure 18: SHAP summary plot for Isolation Forest LSTM for the operation-level dataset.

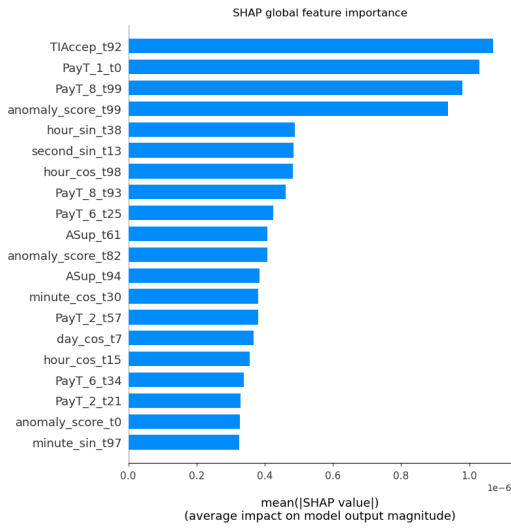


Figure 19: SHAP summary bar plot for Isolation Forest Transformer for the declaration-level dataset.

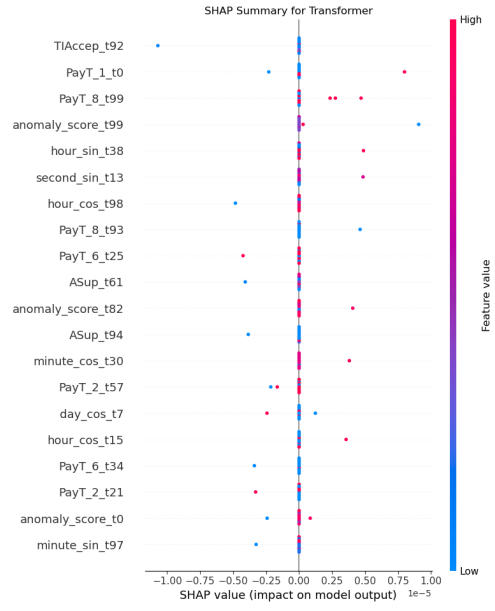


Figure 20: SHAP summary plot for Isolation Forest Transformer for the declaration-level dataset.

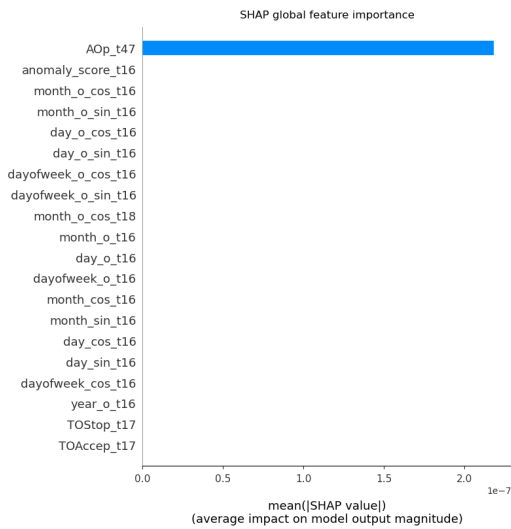


Figure 21: SHAP summary bar plot for Isolation Forest Transformer for the operation-level dataset.

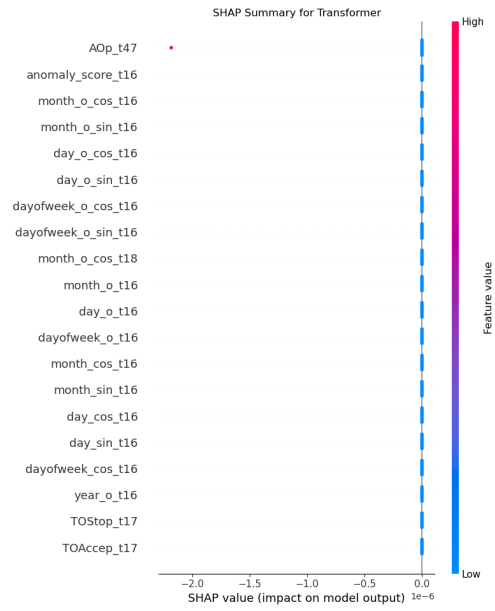


Figure 22: SHAP summary plot for Isolation Forest Transformer for the operation-level dataset.

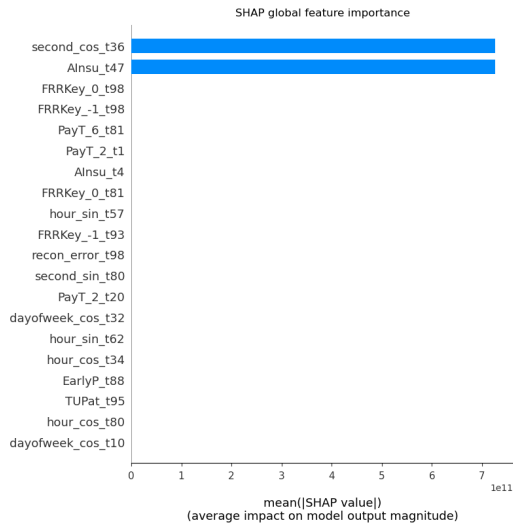


Figure 23: SHAP summary bar plot for Autoencoder LSTM for the declaration-level dataset.

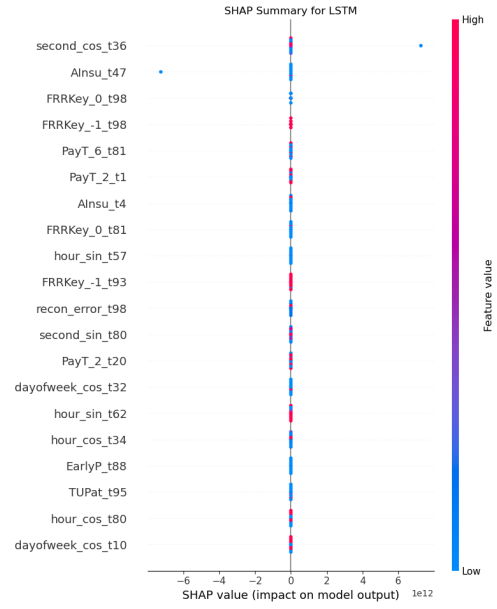


Figure 24: SHAP summary plot for Autoencoder LSTM for the declaration-level dataset.

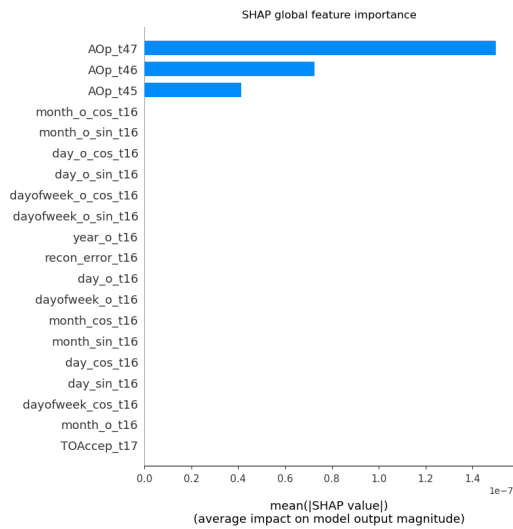


Figure 25: SHAP summary bar plot for Autoencoder LSTM for the operation-level dataset.

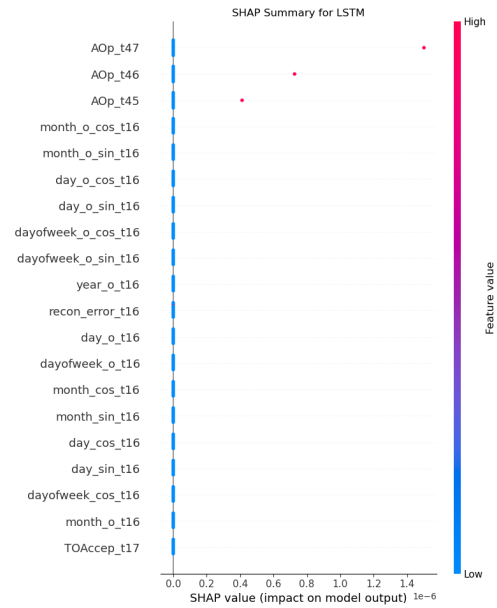


Figure 26: SHAP summary plot for Autoencoder LSTM for the operation-level dataset.

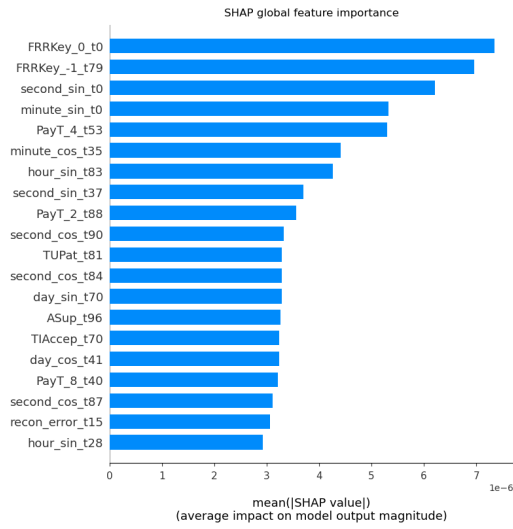


Figure 27: SHAP summary bar plot for Autoencoder Transformer for the declaration-level dataset.

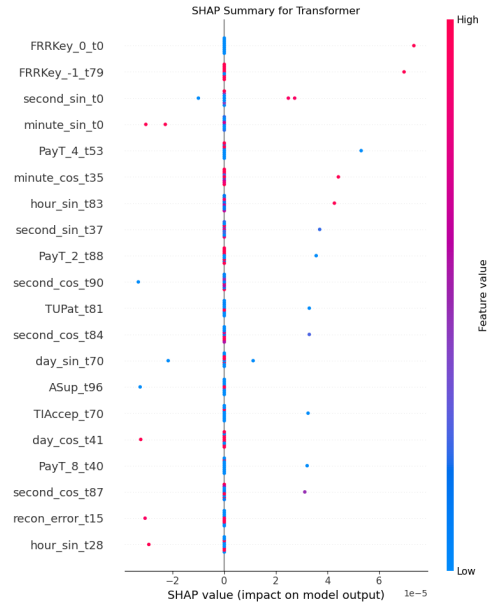


Figure 28: SHAP summary plot for Autoencoder Transformer for the declaration-level dataset.

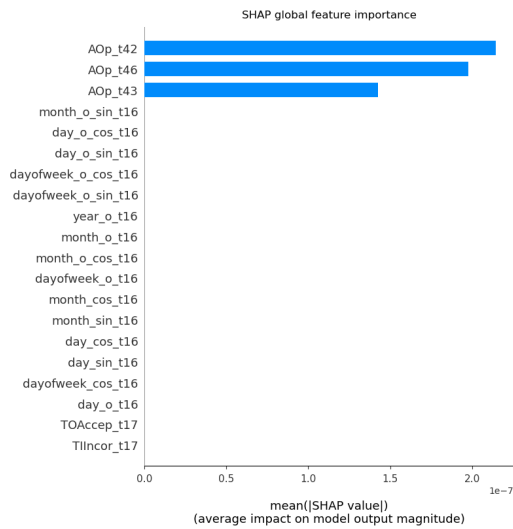


Figure 29: SHAP summary bar plot for Autoencoder Transformer for the operation-level dataset.

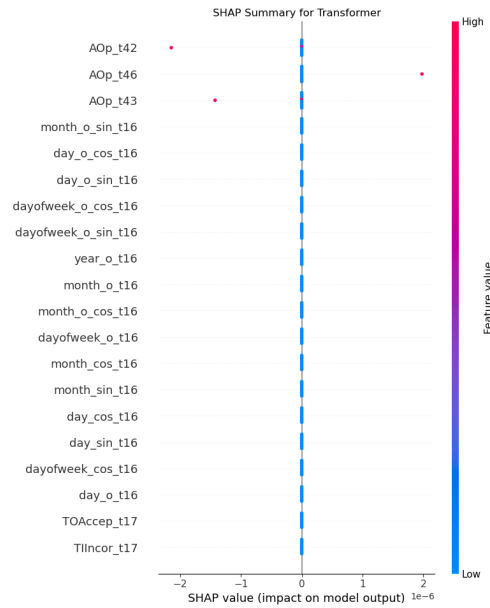


Figure 30: SHAP summary plot for Autoencoder Transformer for the operation-level dataset.

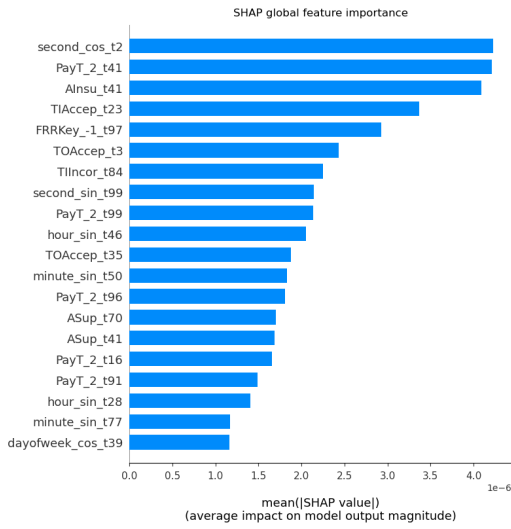


Figure 31: SHAP summary bar plot for original-label LSTM for the declaration-level dataset.

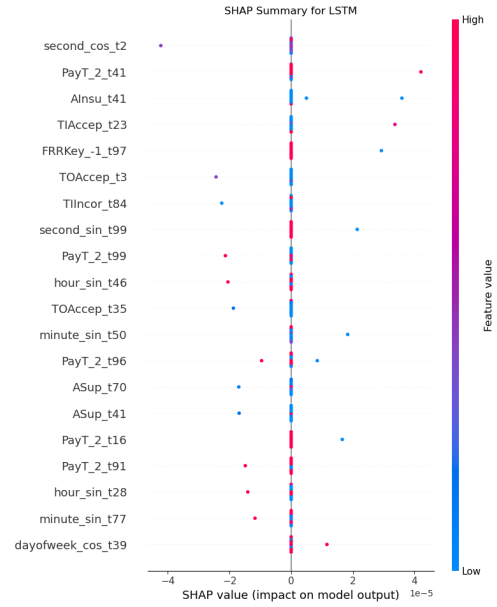


Figure 32: SHAP summary plot for original-label LSTM for the declaration-level dataset.

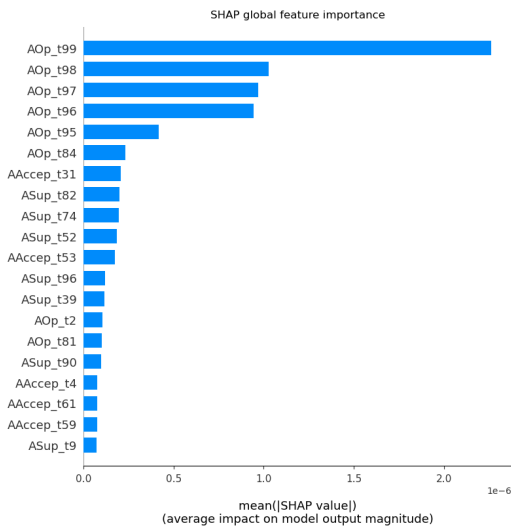


Figure 33: SHAP summary bar plot for original-label LSTM for the operation-level dataset.

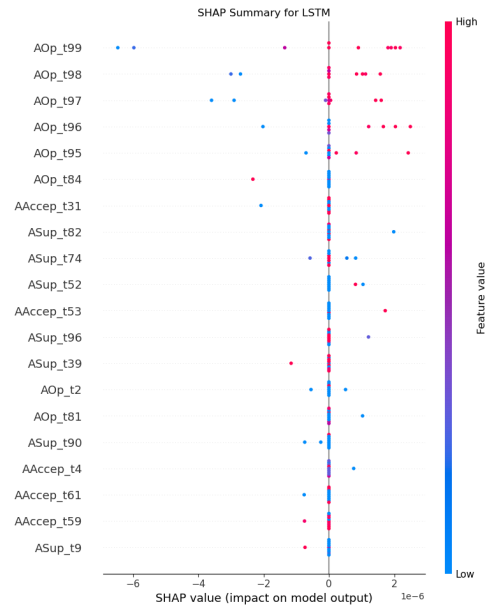


Figure 34: SHAP summary plot for original-label LSTM for the operation-level dataset.

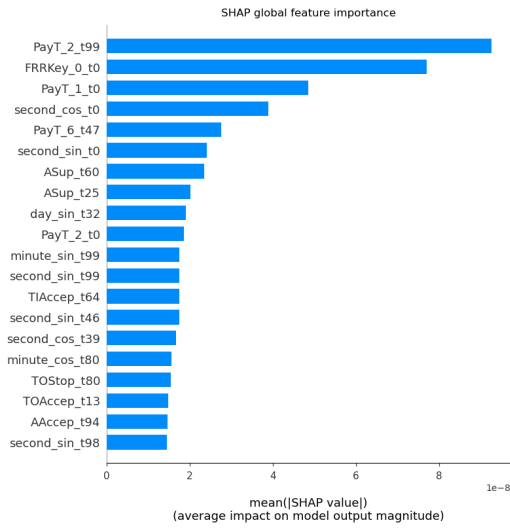


Figure 35: SHAP summary bar plot for original-label Transformer for the declaration-level dataset.

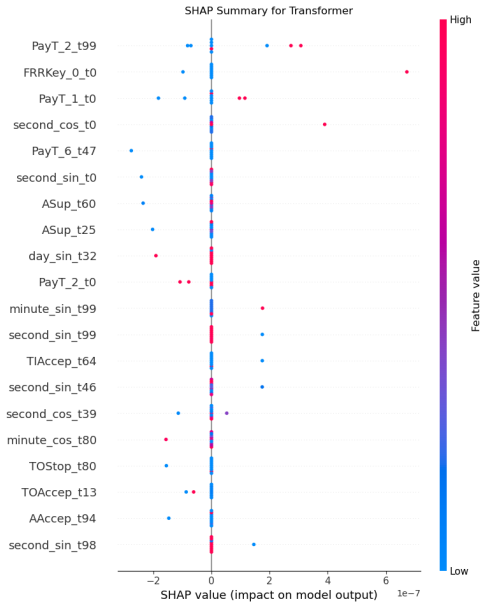


Figure 36: SHAP summary plot for original-label Transformer for the declaration-level dataset.

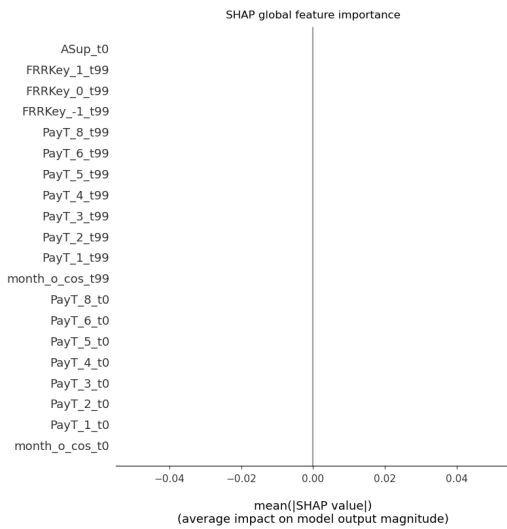


Figure 37: SHAP summary bar plot for original-label Transformer for the operation-level dataset.

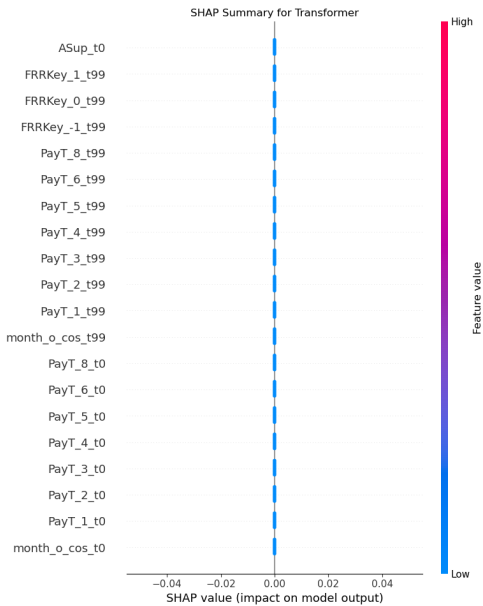


Figure 38: SHAP summary plot for original-label Transformer for the operation-level dataset.